CrossMark

ORIGINAL PAPER

Qualitative Evaluation of Ultra-thin Multi-layer Diamond-Like Carbon Coatings Using Molecular Dynamics Nanoindentation Simulations

Michael R. Price[1] · Andrey Ovcharenko[2] · Bart Raeymaekers[1]

Abstract Ultra-thin diamond-like carbon (DLC) coatings are used in hard disk drives to protect the intricate magnetic structures from wear and corrosion. The coating on the recording head consists of a hard DLC layer and a silicon (Si) layer that improves adhesion between the DLC layer and the substrate. Damage to this protective coating can expose the magnetic structures to corrosion and compromise the reliability and functionality of the hard disk drive. Hence, it is critical to understand how coating design parameters affect the mechanical properties of these protective DLC coatings. We have used molecular dynamics simulations to determine the hardness and Young's modulus of the ultra-thin multi-layer protective DLC coating of a recording head as a function of coating design parameters. We have found that hardness and Young's modulus of the multi-layer coating increase with increasing DLC layer and decreasing Si layer thickness. Furthermore, hardness and Young's modulus of the multi-layer coating are a function of the sp^3 fraction and, thus, the hardness of the DLC layer. In addition, the mismatch between the hardness of the DLC layer and the substrate determines whether plastic deformation occurs in the coating or the substrate, and significantly affects the hardness of the multi-layer protective coating.

Keywords Nanoindentation · Molecular dynamics · Diamond-like carbon · Hard disk drive · Ultra-thin films

✉ Bart Raeymaekers
bart.raeymaekers@utah.edu

[1] Department of Mechanical Engineering, University of Utah, Salt Lake City, UT 84112, USA

[2] Western Digital Corporation, San Jose, CA 95138, USA

1 Introduction

Increasing the storage density of a hard disk drive (HDD) requires decreasing the magnetic spacing between the recording head and the magnetic disk to improve magnetic coupling and enable writing and reading increasingly small bits [1, 2]. An ultra-thin diamond-like carbon (DLC) overcoat protects the delicate magnetic structures of the recording head from accidental contact with the disk. In addition, a Si, SiN, or Cr layer often strengthens adhesion between the DLC layer and the substrate of the recording head, and improves wear resistance of the coating [3]. Reducing the magnetic spacing involves decreasing the thickness of the ultra-thin protective overcoat, which may reduce its strength and wear resistance. Consequently, damage to or removal of the DLC coating, even in part, may expose the read/write structures to corrosion and compromise their reliability and function. Experiments have documented wear and delamination of the protective overcoat, in particular at the pole tip area of the recording head [4].

To prevent wear and delamination of the protective overcoat, it is important to understand its mechanical properties as a function of coating design parameters, including thickness and sp^3 fraction of the DLC layer, and the thickness of the Si layer. Mechanical properties of thin coatings are typically determined using nanoindentation. Indenting a surface with a hard tip while monitoring the force as a function of indentation depth enables calculating the hardness and Young's modulus of the material [5]. Hardness relates to the wear resistance of a material [6, 7]. Several researchers have used nanoindentation to study the mechanical properties of DLC coatings. Sui and Cai [8] found that lowering the sp^3/sp^2 ratio of the DLC coating reduces hardness, whereas Beake and Lau [9] documented

that increasing the thickness of a DLC coating increases hardness, similar to the findings of Ma et al. [10]. However, the thickness of the DLC coatings evaluated in these studies is on the order of 80 nm, which significantly exceeds the thickness of DLC coatings currently used in HDDs. Other researchers have focused specifically on evaluating the mechanical properties of DLC coatings used on magnetic disks. For instance, Lee et al. [7] measured the hardness and Young's modulus of sub-10-nm DLC coatings on magnetic disks and found that the mechanical properties measured near the surface are significantly affected by the coating layers below the DLC layer. Li and Bhushan [11] also found that the mechanical properties of magnetic disks depend on indentation depth due to the layered structure of the DLC and magnetic coatings. Hence, to reliably measure nanoscale mechanical properties of thin coatings, the indentation depth should not exceed 10–20 % of the coating thickness [12]. As the thickness of DLC coatings in state-of-the-art HDDs approaches one to several nanometers, it becomes increasingly difficult to experimentally measure their mechanical properties. Thus, simulation tools such as molecular dynamics (MD) have gained attention to evaluate the mechanical and tribological properties of ultra-thin coatings [13, 14].

Several publications document using MD to simulate nanoindentation of crystalline [15, 16] and non-crystalline [17–20] materials, although quantifying deformation remains difficult in amorphous materials due to the lack of an atomistic model for plastic flow [13]. Slufarzka et al. [17, 18] modeled nanoindentation of amorphous SiC and found that nanoindentation damage is less localized in amorphous SiC than in cubic SiC and that inception of plastic deformation during nanoindentation occurs closer to the surface in the former than in the latter. Sinnot [19] simulated nanoindentation of DLC and found that the Young's modulus is in good agreement with experimental measurements. Wang and Komvopoulos [20] also modeled nanoindentation of DLC and found that for indentations of <1 nm, the critical coating thickness for avoiding substrate effects is 3.5 nm. However, the small size and time scales of MD simulations in addition to simplified material models often limit MD results to describe qualitative behaviors and trends rather than reproduce exact experimental results [13].

While critical to the design of ultra-thin protective coatings for magnetic recording heads, no studies exist to the best of our knowledge that systematically evaluate and describe the effect of different coating parameters on the nanoscale mechanical properties of the multi-layer coating of a magnetic recording head in a HDD. Hence, the objective of this paper is to determine the effect of coating design parameters, including thickness and composition, on

the mechanical properties of the multi-layer protective coating of a magnetic recording head using nanoindentation simulations. This knowledge enables optimizing the coating parameters in terms of, e.g., maximum hardness or stiffness for a given thickness budget of the entire multi-layer coating, and it allows deriving coating design guidelines for minimizing plastic deformation of the coating or substrate due to accidental contact with the disk. Although the emphasis of this paper is on magnetic recording heads used in HDDs, the results are relevant for any system in which the qualitative effect of coating design parameters on the mechanical properties of a multi-layer coating must be understood.

2 Methods

2.1 Model

Figure 1a shows a schematic of a section of the head/disk interface near the pole tip area of the recording head, where wear and delamination of the DLC coating typically occurs [4]. Figure 1b shows the molecular dynamics model of a small section of the top pole, as indicated by the rectangular box in Fig. 1a.
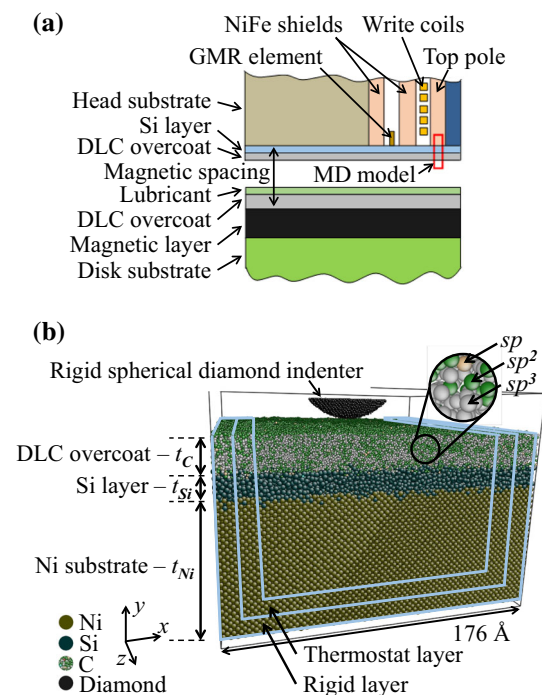

Fig. 1 a Schematic of a portion of the recording head and magnetic disk in a hard disk drive. b Molecular dynamics model of a small portion of the recording head, indicated by the *red rectangular box* in a (Color figure online)

The MD model of the recording head consists of a bulk Ni substrate of thickness $t_{Ni} = 70$ Å, covered with a DLC layer of thickness 12 Å $\leq t_C \leq 18$ Å. An amorphous Si layer of thickness 3 Å $\leq t_{Si} \leq 9$ Å improves adhesion between the DLC layer and Ni substrate. We have used Ni as the shield substrate material of the recording head instead of NiFe to simplify the computational model. Although the magnetic properties of NiFe and Ni are different, the mechanical properties such as hardness, Young's modulus, and Poisson ratio, which are of primary interest in this study, are similar [21–24]. The Si and DLC layers together comprise the protective coating, maintained at a combined thickness of $t_C + t_{Si} = 21$ Å throughout this study. The fraction of sp^3-hybridized carbon atoms in the DLC layer on a recording head is approximately 70 % (tetrahedral amorphous carbon, ta-C) [24]. However, to investigate the effect of the sp^3 fraction of the DLC layer on the mechanical properties of the protective coating, we perform the simulations for a DLC layer with 30 % (amorphous carbon, a-C), 50 %, and 70 % (ta-C) sp^3 fraction. We model the indenter as a rigid spherical tip with a radius of 35 Å, which is 20 % of the 176 Å $\times$ 120 Å $\times$ 176 Å simulation box, chosen after a convergence study of the effect of box size and tip radius on the resulting mechanical properties. The model contains between 250,000 and 350,000 atoms, depending on t_{Si}, t_C, and sp^3 fraction of the DLC layer.

We create the MD model using a multi-step annealing procedure, similar to the single-step annealing procedure used in other MD simulations of DLC [20, 25]. We first create separate layers of DLC (30 Å) and amorphous Si (20 Å) by heating carbon and silicon atoms to 6000 and 4000 K, respectively, and increasing the pressure to obtain the desired sp^3 fraction. We subsequently quench the amorphous phase to 300 K. We then place the amorphous Si layer between the DLC layer and the (100) plane of the Ni substrate and use a similar annealing procedure at the DLC–Si and Si–Ni interfaces. We remove the middle segments of the DLC and amorphous Si layers to decrease the thickness of each respective layer to the desired value of t_C and t_{Si}, and to ensure that all simulations will initiate from the same surface topography of the DLC coating. Finally, we bring the surfaces exposed by the removal of the middle of the DLC and Si layers into contact, and perform a final annealing procedure of the atomic layers nearest the exposed atoms. Using this multi-step annealing procedure, the atomic structure of the DLC surface and the interfaces between the layers are the same for different coatings and, thus, the simulation results are only dependent on t_C and t_{Si} and not the local atomic structure of the interfaces between the different material layers and the DLC surface topography.

We have used the following interatomic potentials: MEAM [26, 27] for Ni–Ni and Ni–Si interactions, Tersoff [28] for Si–Si, Si–C and C–C interactions, and 12-6 Lennard-Jones potential truncated at the zero-energy distance for the interactions between the indenter tip and the recording head so that we only consider repulsive interactions, simulating an indentation that neglects adhesion [29]. We use $\sigma = 1.5$ Å for the LJ parameter that represents the length of a bond between sp^2- and sp^3-hybridized carbon atoms [30]. Because the LJ potential is truncated at 1.5 Å, the results from the nanoindentation simulations are not sensitive to the LJ energy parameter ε, which we have set $\varepsilon = 1$ eV.

We use the Sandia LAMMPS code to perform the nanoindentation simulations [31]. We hold the outer three atomic layers of the Ni substrate rigid and we maintain the three atomic layers immediately inward from the rigid layers at 300 K using a Langevin thermostat to simulate the presence of bulk material around the simulation box (see Fig. 1b). The remaining atoms are free to move according to classical mechanics and the microcanonical ensemble. We maintain a time step of 0.25 fs throughout this work and perform equilibration at 300 K for 10 ps prior to all simulations.

2.2 Simulation Procedure

Figure 2a shows the indentation depth h versus time t of the nanoindentation procedure described by Oliver and Pharr [5], applied to a picosecond time scale. The purpose of the multiple load-unload cycle is to ensure that the unloading data used in the analysis are mostly elastic. However, due to the high computational cost of MD simulations, we use a modified nanoindentation procedure based on a single load and unload cycle as shown in Fig. 2b, and similar to what others have used [29, 32]. We have determined a difference of <6 % between the hardness and Young's modulus obtained with both nanoindentation procedures, indicating that using a single-cycle procedure minimally affects the nanoindentation results for the coatings we have evaluated.

We perform indentation simulations of 3 Å $\leq h \leq 13$ Å deep, which does not exceed 13 % of the thickness of the multi-layer coating and non-rigid substrate atoms, to avoid that the rigid substrate atoms influence the results [12]. However, because the indentation depth significantly exceeds 10 % of the thickness of the DLC layer, the results represent the mechanical properties of the entire multi-layer coating and substrate, instead of the DLC layer by itself. The indenter moves with velocity $v_y = 50$ m/s as it follows the prescribed loading curve (Fig. 2b), which is higher than in physical nanoindentation experiments, but is typical of nanoindentation simulations as discussed by,
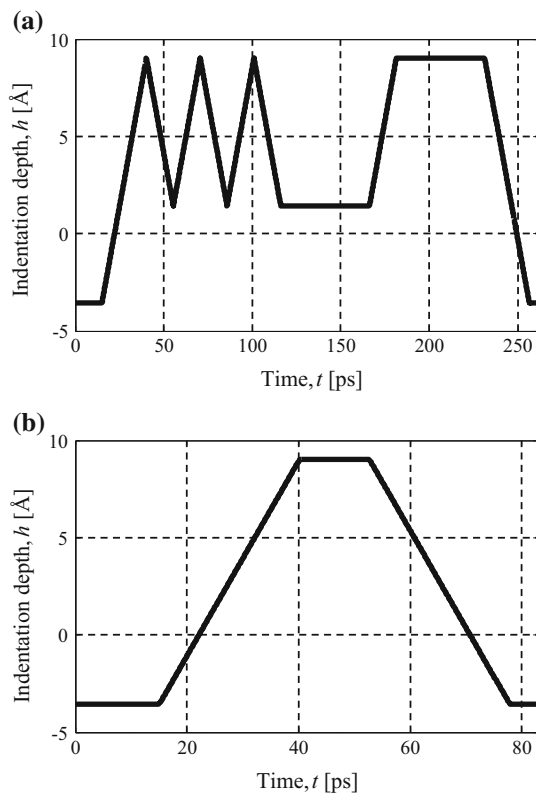
(a)

(b)

Fig. 2 Nanoindentation procedure showing indentation depth as a function of time for **a** the Oliver and Pharr method [5] applied to a picosecond time scale and **b** the modified method used in this study

(a)

(b)

Fig. 3 a Typical nanoindentation force versus indentation depth curve for a coating with $t_{Si} = 6$ Å and $t_C = 15$ Å (70 % sp^3 fraction). The *solid black line* shows the curve-fit to the unloading portion of the curve. The *dashed black line* is the tangent line to the unloading curve at (h_{max}, P_{max}) used to determine the contact depth h_c. **b** Schematic showing contact depth h_c, indentation depth h, and contact radius r_c

e.g., Noreyan et al. [32] and Nair et al. [33], who showed that the indentation velocity has a negligible effect on the results of MD nanoindentation simulations within the range of velocities used in their studies (2.5–85.7 m/s).

2.3 Data Analysis

Figure 3a shows a typical force P versus indentation depth h result for a coating with $t_{Si} = 6$ Å and $t_C = 15$ Å (70 % sp^3 fraction). First, we fit $P = C(h - h_f)^m$ to the unload portion of the curve where C, h_f, and m are curve-fit parameters determined using the least-squares method (curve-fit shown as black solid curve). Then, we calculate the hardness $H = P_{max}/A$ and Young's modulus $E = S/2 \cdot (\pi/A)^{1/2}$, where A is the projected contact area between the indenter and the coating and $S = dP/dh$ is the unloading stiffness at the inception of unloading (h_{max}, P_{max}). The dashed black line is the tangent line to the unloading curve at (h_{max}, P_{max}), which we use together with an indenter tip geometry shape factor [5] to determine the contact depth h_c and the projected contact area A. Figure 3b schematically illustrates the difference between the contact depth h_c and the indentation depth h, and defines the relationship between contact radius r_c and contact depth
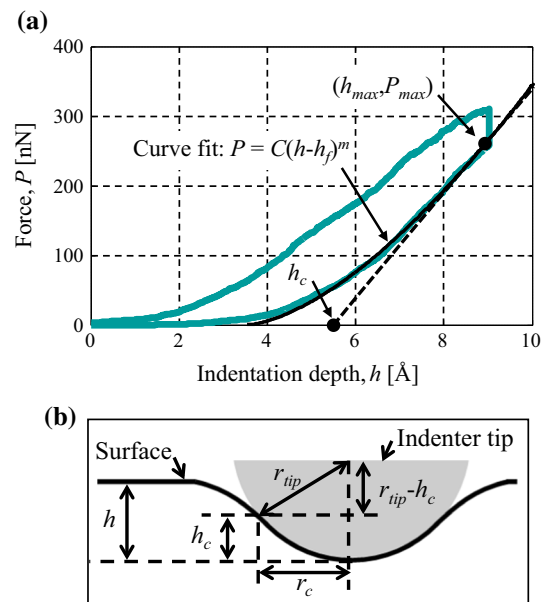
h_c as $r_c = [(r_{tip}^2 - (r_{tip} - h_c)^2]^{1/2}$. Contact occurs when a coating atom experiences a nonzero force due to the presence of the indenter. We use the tangent line to the unloading curve to determine h_c (see Fig. 3) and calculate the projected contact area $A = \pi r_c^2$. This method yields similar results than determining A directly from atomic coordinates but allows a continuous rather than discrete possible outcome for the measurement of A, and avoids inaccuracies introduced by, e.g., fitting a minimum bounding circle to the contacting atoms.

2.4 Deformation Characterization

We quantify deformation of the multi-layer coating and substrate by measuring the displacement of individual atoms d_i, relative to their initial positions, throughout the nanoindentation simulation. Figure 4 shows the atomic displacement in a plane of atoms along the centerline of the indenter, for a coating with $t_{Si} = 6$ Å and $t_C = 15$ Å (70 % sp^3 fraction), at an indentation depth of 9 Å. The displacement d_i of each atom is represented by an arrow, whose direction and length represent the direction and magnitude of the displacement, respectively. We observe that the displacement of the atoms in the amorphous DLC and Si layers is radially symmetric about the center axis of the indenter tip, whereas the displacement of the Ni atoms is preferential to the <110> directions because of its face-
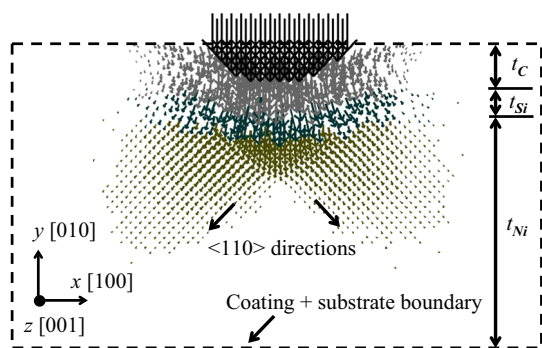
Fig. 4 Displacement d_i of atoms during indentation, at maximum indentation depth of 9 Å, of a coating with $t_{Si} = 6$ Å and $t_C = 15$ Å (70 % sp^3 fraction), shown as an *arrow* with length and thickness corresponding to the magnitude of d_i

Table 1 Simulated hardness and Young's modulus of the individual materials that comprise the multi-layer coating of the recording head in a HDD

Material	Hardness (GPa)	Young's modulus (GPa)
Ni (100)	20	202
a-Si	9	157
ta-C (70 % sp^3 fraction)	195	1221
a-C (30 % sp^3 fraction)	120	788

centered cubic (FCC) lattice. Some of the deformation caused by indentation is elastic and recovered upon unloading; the remainder is plastic. We quantify the plastic zone size as the fraction of atoms in each material layer of the coating and substrate (f_C, f_{Si}, and f_{Ni}) that undergo permanent displacement due to indentation. By comparing the coordinates of each atom at the initial time step of the simulation with those at a later time step but before indentation, we determine the probability density function (PDF) of the atomic displacement of each atom type due only to thermal motion. By comparing the PDFs before and after indentation, we determine the fraction of atoms that have moved further than what is expected due to thermal motion. Hence, this method distinguishes between atomic displacement resulting from thermal motion and that caused by indentation, and it does not rely on a cutoff distance to determine plastic deformation as in, e.g., [17], which does not account for small permanent displacement of atoms. Furthermore, the area under the force versus indentation depth loading curve represents the indentation energy e_{ind}, whereas the area contained between the loading and unloading curves represents the portion of the indentation energy that causes plastic deformation e_{pl} (see Fig. 3a). Hence, e_{pl}/e_{ind} quantifies the amount of plastic relative to total deformation [34].

3 Results and Discussion

We have performed nanoindentation simulations of bulk Ni, a-Si, and DLC with 30 % (a-C) and 70 % (ta-C) sp^3 fraction, using the procedure described in Sect. 2.2. Table 1 shows the simulated hardness and Young's modulus of the bulk materials, which, although higher than experimental results for Ni, ta-C, and a-C, are in good agreement with other simulation results [18, 35–38]. The results of MD simulations are limited by the accuracy of

the interatomic potentials used to describe the materials, and by the time scale and spatial domains that can be resolved.

We have also performed nanoindentation simulations of three different multi-layer coatings (70 % sp^3 fraction DLC layer and Si layer) on a Ni substrate using the procedure described in Sect. 2.2. Figure 5a shows a schematic of the three coatings with varying t_C and t_{Si} but constant total coating thickness $t_C + t_{Si} = 21$ Å. Figure 5b shows the hardness H and Fig. 5c shows the Young's modulus E of the multi-layer coatings as a function of indentation depth h. The hardness and Young's modulus of the multi-layer coating approaches those of bulk Ni with increasing indentation depth because the properties of the Ni substrate increasingly dominate the measurement, in agreement with [11, 39, 40]. We also observe that hardness and Young's modulus increase with increasing t_C, in agreement with experimental results [8, 9]. This is because the DLC layer has the highest hardness and Young's modulus of the three materials (see Table 1), and, therefore, its effect on hardness and Young's modulus of the multi-layer coating increases with increasing thickness. Furthermore, the hardness and Young's modulus decrease with increasing t_{Si}, because the Si layer has the lowest hardness and Young's modulus of the three materials (see Table 1) and the increasing Si layer thickness comprises an increasing fraction of the total thickness of the multi-layer coating. The hardness depends on t_C and t_{Si} for all indentation depths because hardness measurements for hard-on-soft coatings are affected by the substrate when the indentation depth is greater than 10 % of the thickness of the coating, or when the hardness mismatch between coating and substrate causes yielding of the substrate before yielding of the coating [12]. This is in qualitative agreement with the experimental results of Lee et al. [7] for nanoindentation of DLC-coated magnetic disks.

To quantify the effect of the stochastic nature of MD simulations on the results, we have performed twelve separate indentations of the coating with $t_C = 15$ Å, $t_{Si} = 6$ Å, $h_{max} = 9$ Å, and 70 % sp^3 fraction DLC layer, which is an intermediate case of the parameter ranges
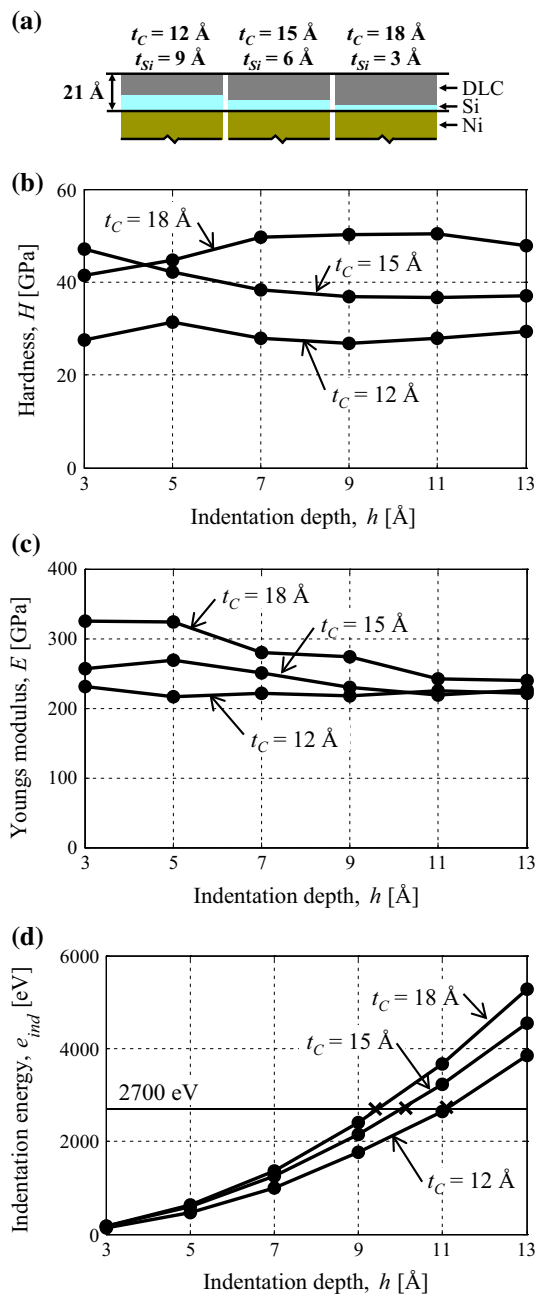
(a)

(b)

(c)

(d)

Fig. 5 **a** Schematic of three coatings with varying t_C and t_{Si} and with constant total coating thickness, and **b** hardness H, **c** Young's modulus E, and **d** indentation energy e_{ind} as a function of indentation depth for the coatings shown in **a** with 70 % sp^3 fraction DLC

shown in Fig. 5. We have varied the initial distribution of atomic positions and velocities, and remade the multi-layer coating using the procedure described in Sect. 2.1 to vary the surface topography of the amorphous DLC coating. We find that the coefficient of variation of the hardness and Young's modulus is 7.3 and 3.4 %, respectively. In addition, we have performed a similar analysis of the same coating for the shallowest indentation depth $h_{max} = 3$ Å,

and find a coefficient variation of 15.5 and 1.7 % for hardness and Young's modulus, respectively. The increased coefficient of variation for the shallowest indentation is because the indentation force decreases with decreasing indentation depth, thus reducing the signal-to-noise ratio. From this analysis, we conclude that the variation of the results due to the stochastic nature of MD is smaller than the differences in hardness and Young's modulus results for the different coatings shown in Fig. 5b, c, except for the hardness determined for the shallowest indentation depths.

Figure 5d shows the indentation energy e_{ind} as a function of the indentation depth h. We observe that the indentation energy increases with increasing indentation depth because more material must be displaced. Additionally, the indentation energy increases with increasing t_C and decreasing t_{Si} for constant indentation depth because of the increasing hardness of the multi-layer coating. Thus, we will evaluate plastic deformation of the coatings of Fig. 5a for (1) constant indentation depth, and (2) for constant indentation energy. We have chosen an indentation energy $e_{ind} = 2700$ eV, indicated by a horizontal line in Fig. 5d, in the middle of the range we have investigated.

Figure 6a–c shows the fraction of permanently displaced C (f_C), Si (f_{Si}), and Ni (f_{Ni}) atoms after indentation of the three multi-layer coatings shown in Fig. 5a as a function of indentation depth h. Analogous to the analysis of the data in Fig. 5, we compute the coefficient of variation of f_C, f_{Si}, and f_{Ni} to be 4.6, 2.6, and 9.6 %, respectively. We observe that f_C, f_{Si}, and f_{Ni} increase with increasing indentation depth, f_C increases with decreasing DLC layer thickness t_C, and f_{Si} and f_{Ni} are nearly independent of t_C. Because the hardness of the DLC layer decreases with decreasing t_C (see Fig. 5b), it provides less resistance to plastic deformation [41]. This is in agreement with the experimental results of Yasui et al. [39] that show increasing hardness and decreasing plastic deformation of DLC-coated magnetic media with increasing DLC layer thickness. Figure 6d shows the contour of the DLC layer of the three coatings after indentation with $h_{max} = 5$ and 13 Å, respectively, illustrating that the increase in plastic deformation of the DLC layer f_C with decreasing t_C and increasing indentation depth results from the indenter beginning to penetrate through the DLC layer rather than bending or compressing it.

Figure 7a shows the fraction of permanently displaced C (f_C), Si (f_{Si}), and Ni (f_{Ni}) atoms after indentation with a constant indentation energy $e_{ind} = 2700$ eV as a function of DLC layer thickness t_C. Figure 7b shows the contour of the DLC layer after indentation with $e_{ind} = 2700$ eV, indicating the depth of the permanent indentation depression d_{pl}, and Fig. 7c shows the depth of the permanent indentation depression d_{pl} and the fraction of indentation
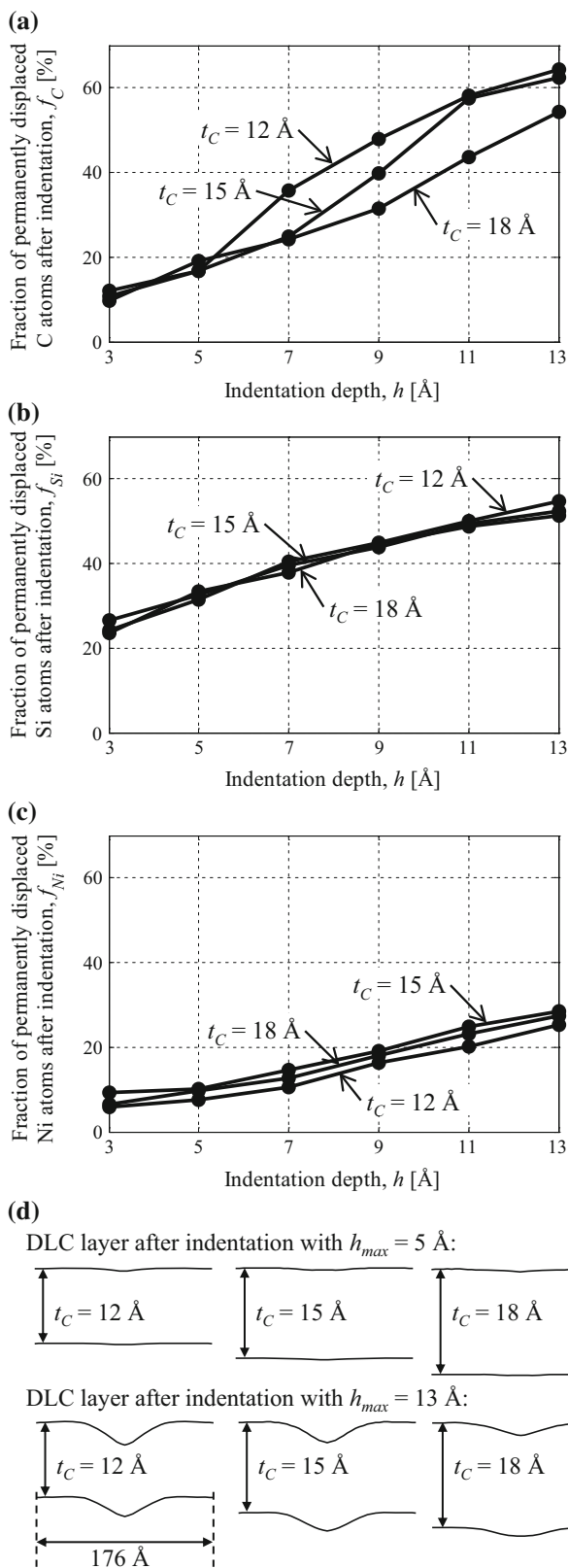
(a)

(b)

(c)

(d)

DLC layer after indentation with $h_{max} = 5$ Å:

DLC layer after indentation with $h_{max} = 13$ Å:

Fig. 6 Fraction of permanently displaced **a** C atoms f_C, **b** Si atoms f_{Si}, and **c** Ni atoms f_{Ni} after indentation as a function of indentation depth h for the three multi-layer coatings of Fig. 5a, and **d** contour of DLC layer after indentation with $h_{max} = 5$ and 13 Å
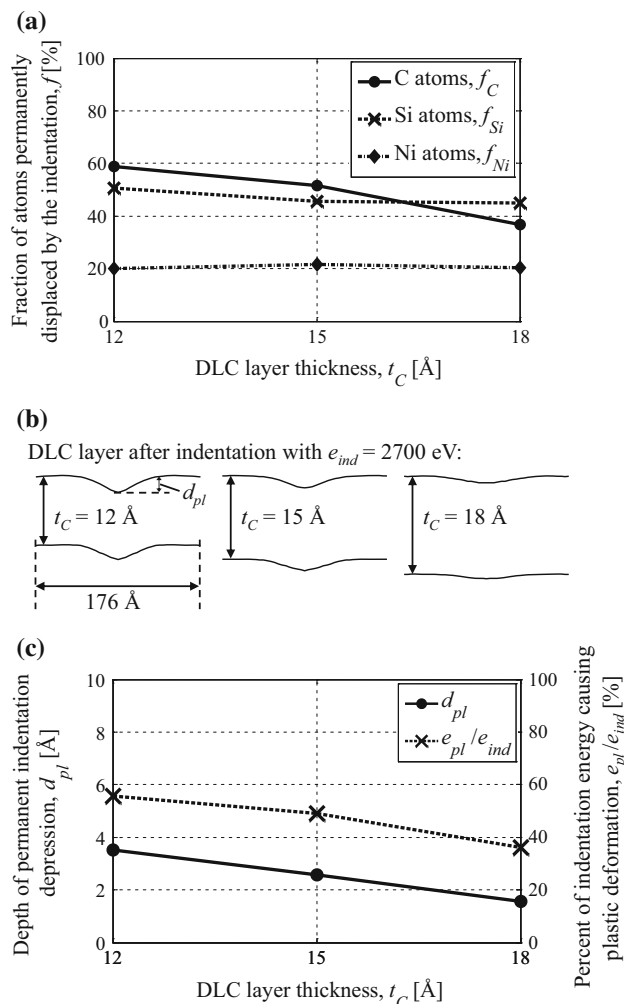
(a)

(b)

DLC layer after indentation with $e_{ind} = 2700$ eV:

(c)

Fig. 7 a Fraction of permanently displaced C (f_C), Si (f_{Si}), and Ni (f_{Ni}) atoms after indentation, **b** the contour of the DLC layer of each coating after indentation, and **c** the depth of the permanent indentation depression d_{pl} and the percent of indentation energy causing plastic deformation e_{pl}/e_{ind} as a function of the DLC layer thickness t_C for indentations with constant indentation energy $e_{ind} = 2700$ eV

energy causing plastic deformation e_{pl}/e_{ind} as a function of t_C for constant indentation energy $e_{ind} = 2700$ eV.

From Fig. 7a, we observe that the fraction of C (f_C) and Si (f_{Si}) atoms permanently displaced by the indentation decreases with increasing t_C. In addition, from Fig. 7b, c we observe that the fraction of the indentation energy causing plastic deformation decreases with increasing t_C, which results in decreasing depth of the permanent depression after indentation d_{pl}. Hence, for a constant total coating thickness budget, increasing the fraction of the coating comprised of DLC and decreasing the fraction comprised of Si will decrease plastic deformation in the coating resulting from an accidental contact between the recording head and magnetic disk, because the hardness of the coating increases. These results are in agreement with

experimental results that document decreasing hardness with decreasing DLC layer thickness (e.g., [39]). We also observe that f_{Ni} is nearly independent of t_C because the coating thickness and indentation energy are constant and the indenter tip remains distant (>8 Å, or 40 % of the total coating thickness) from the Ni substrate for all indentations.

Figure 8a, b shows the hardness H and Young's modulus E of the multi-layer coating, respectively, as a function of the sp^3 fraction of the DLC layer, for the three different multi-layer coatings of Fig. 5a, and for constant indentation energy $e_{ind} = 2700$ eV. From Fig. 8, we observe that H and E first increase and then decrease with increasing sp^3 fraction of the DLC layer for the coatings investigated. This is different from the mechanical properties of DLC by itself, for which H and E increase monotonically with increasing sp^3 fraction (see Table 1 and [40]). We clarify this as follows. H and E of the multi-layer coating increase with increasing H and E of a DLC layer of constant thickness t_C and, thus, with increasing sp^3 fraction of the DLC layer. However, with increasing mismatch between the mechanical properties of the DLC layer and the material layers underneath, plastic deformation is increasingly preferential to the soft Si layer and Ni substrate, and
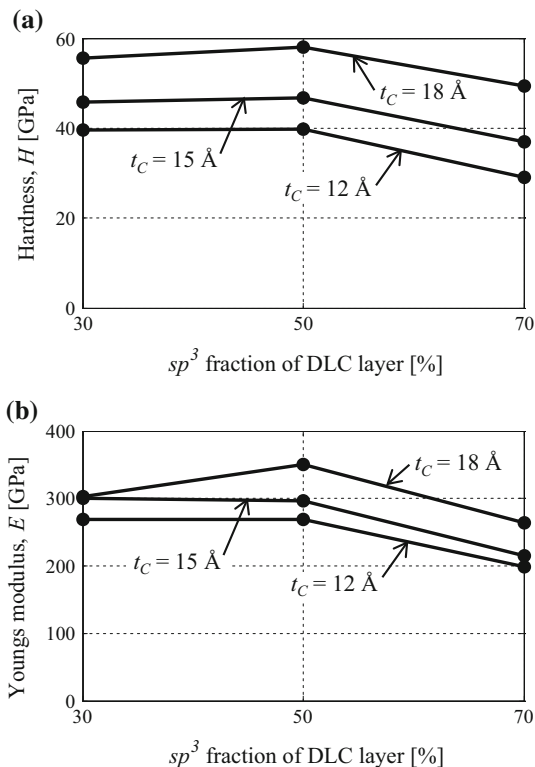

(a)

(b)

Fig. 8 **a** Hardness and **b** Young's modulus as a function of sp^3 fraction of the DLC layer and coating parameter t_C. Results are shown for constant indentation energy $e_{ind} = 2700$ eV and constant total coating thickness $t_C + t_{Si} = 21$ Å

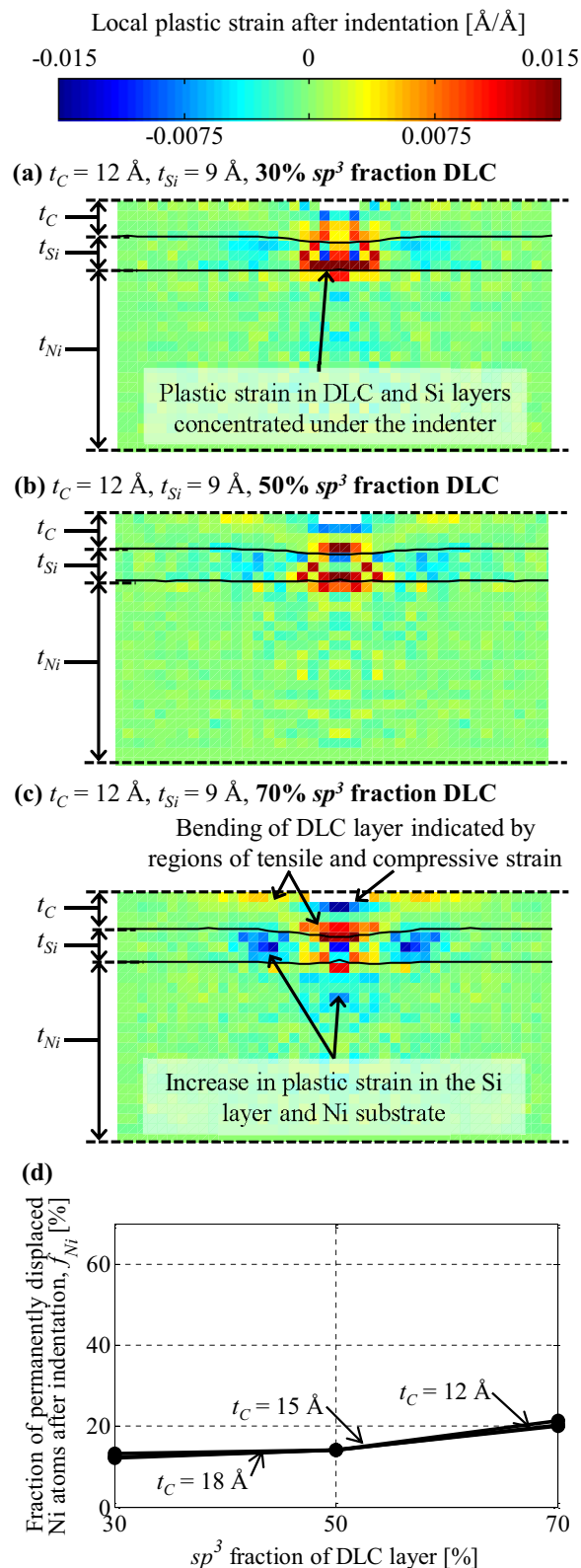Local plastic strain after indentation [Å/Å]

(a) $t_C = 12$ Å, $t_{Si} = 9$ Å, **30% sp^3 fraction DLC**

Plastic strain in DLC and Si layers concentrated under the indenter

(b) $t_C = 12$ Å, $t_{Si} = 9$ Å, **50% sp^3 fraction DLC**

(c) $t_C = 12$ Å, $t_{Si} = 9$ Å, **70% sp^3 fraction DLC**

Bending of DLC layer indicated by regions of tensile and compressive strain

Increase in plastic strain in the Si layer and Ni substrate

(d)

Fig. 9 Local plastic strain after indentation of the multi-layer coating with $t_C = 12$ Å and $t_{Si} = 9$ Å and **a** 30 %, **b** 50 %, and **c** 70 % sp^3 fraction DLC, and **d** fraction of permanently displaced Ni atoms after indentation as a function of sp^3 fraction of the DLC layer. Constant indentation energy $e_{ind} = 2700$ eV is maintained

the hard DLC layer bends into the fully plastic substrate [42] rather than being locally compressed under the indenter. This behavior has also been observed experimentally for nanoindentation [43] and scratch [44] tests, in which a diamond tip causes more local plastic deformation in sp^2-rich than in sp^3-rich DLC coatings of the same thickness, because plastic deformation of the substrate underneath the hard (sp^3-rich) coating causes the coating to bend into the substrate rather than being deformed by the indenter [44]. Figure 9 substantiates these observations.

Figure 9a–c shows the local plastic strain in the multi-layer coating with $t_C = 12$ Å and $t_{Si} = 9$ Å after indentation with $e_{ind} = 2700$ eV, for a DLC coating with 30 % sp^3 fraction (Fig. 9a), 50 % sp^3 fraction (Fig. 9b), and 70 % sp^3 fraction (Fig. 9c). Figure 9d shows the fraction of permanently displaced Ni atoms after indentation as a function of sp^3 fraction of the DLC layer. From Fig. 9a, we observe that the plastic strain in the coating with a DLC layer of 30 % sp^3 fraction occurs primarily in the DLC and Si layers, directly under the indenter tip. Plastic strain in the Si layer and Ni substrate increases with increasing sp^3 fraction of the DLC layer (see Fig. 9b, c). Additionally, from Fig. 9d we observe that f_{Ni} increases due to the increasing plastic strain in the Ni substrate with increasing sp^3 fraction of the DLC layer (Fig. 9a–c). Thus, Fig. 9 further substantiates that plastic deformation is increasingly preferential to the substrate with increasing sp^3 fraction of the DLC coating. This causes the hard coating to bend into the plastically deformed substrate rather than being compressed by the indenter and, thus, results in reduced hardness and Young's modulus. These results are also in qualitative agreement with the results of Chen and Vlassak [41], which show increasing plastic deformation of the substrate with increasing coating hardness for a two-layer, hard-on-soft continuum model.

4 Conclusions

We have simulated nanoindentation of multi-layer coatings consisting of a DLC layer on a Ni substrate, with a thin Si layer to improve adhesion between the DLC layer and Ni substrate. These multi-layer coatings are used to protect the intricate magnetic structures of the recording head of a hard disk drive from accidental impact with the disk.

We conclude that the hardness and Young's modulus of the multi-layer coating increase with increasing DLC layer and decreasing Si layer thickness, similar to experimental results obtained by others. DLC and Si are the hardest and softest materials of the multi-layer coating, respectively, and increasing the thickness of each layer increases its fraction of the total thickness of the multi-layer coating, which correspondingly affects its mechanical properties.

Furthermore, the hardness and Young's modulus of the multi-layer coating are a function of the sp^3 fraction and, thus, the hardness of the DLC layer. However, maximizing the hardness of the multi-layer coating is not sufficient to prevent deformation of the intricate recording structures embedded in the substrate of the recording head. Plastic deformation during indentation increasingly occurs in the Si layer and Ni substrate as opposed to in the DLC layer with increasing hardness of the DLC layer. As the plastically deformed Si and Ni layers are no longer able to support the external indentation load, the hard DLC layer bends into the soft Si layer, which reduces the hardness and Young's modulus of the multi-layer coating.

Hence, to create a multi-layer coating with maximum hardness and Young's modulus for a given thickness budget, we recommend increasing the thickness of the DLC layer, decreasing the thickness of the Si layer, and considering the hardness mismatch between the substrate and DLC layer to avoid that the coatings bend into the plastically deformed substrate. Note that this analysis does not quantify the potential reduction or loss of adhesion between the DLC layer and Ni substrate with decreasing Si layer thickness. Hence, for HDD design the thickness of the DLC and Si layers should be increased and decreased, respectively, until the adhesive properties of the Si layer are compromised. To minimize plastic deformation of the magnetic substrate materials, plastic deformation of the coating should be increased, which can be achieved in part by decreasing the sp^3 fraction of the DLC layer. Decreasing the sp^3 fraction of the DLC layer may, however, decrease the hardness and Young's modulus of the multi-layer coating and, thus, a balance should be found between obtaining the desired hardness and Young's modulus to decrease wear of the coating, and minimizing the plastic deformation of the substrate.

References

1. Fontana, R., Hetzler, S., Decad, G.: Technology roadmap comparisons for tape, HDD, and NAND flash: Implications for data storage applications. IEEE Trans. Magn. **48**, 1692–1696 (2012)
2. Goglia, P., Berkowitz, J., Hoehn, J., Xidis, A., Stover, L.: Diamond-like carbon applications in high density hard disc recording heads. Diam. Relat. Mater. **10**, 271–277 (2001)
3. Sander, P., Kaiser, U., Altebockwinkel, M., Wiedmann, L., Benninghoven, A., Sah, R., Koidl, P.: Depth profile analysis of hydrogenated carbon layers on silicon by x-ray photoelectron spectroscopy, Auger electron spectroscopy, electron energy-loss spectroscopy, and secondary ion mass spectrometry. J. Vac. Sci. Technol., A **5**, 1470–1473 (1987)

4. Song, D., Kvitek, R., Schnur, D.: Inspection of pole tip diamondlike carbon wear due to heater-induced head-disc contact. J. Appl. Phys. **99**, 08N107 (2006)

5. Oliver, W., Pharr, G.: An improved technique for determining hardness and elastic modulus using load and displacement sensing indentation experiments. J. Mater. Res. **7**, 1564–1583 (1992)

6. Archard, J.: Contact and rubbing of flat surface. J. Appl. Phys. **24**, 981–988 (1953)

7. Lee, K., Yeo, C., Polycarpou, A.: Nanomechanical property and nanowear measurements for sub-10-nm thick films in magnetic storage. Exp. Mech. **47**, 107–121 (2007)

8. Sui, J., Cai, W.: Mechanical properties and anti-corrosion behavior of the diamond-like carbon films. Surf. Coat. Tech. **201**, 1323–1327 (2006)

9. Beake, B., Lau, S.: Nanotribological and nanomechanical properties of 5-80 nm tetrahedral amorphous carbon films on silicon. Diam. Relat. Mater. **14**, 1535–1542 (2005)

10. Ma, X., Komvopoulos, K., Wan, D., Bogy, D., Kim, Y.: Effects of film thickness and contact load on nanotribological properties of sputtered amorphous carbon thin films. Wear **254**, 1010–1018 (2003)

11. Li, X., Bhushan, B.: A review of nanoindentation continuous stiffness measurement technique and its applications. Mater. Charact. **48**, 11–36 (2002)

12. Hainsworth, S., Page, T.: Mechanical property data for coated systems—the prospects for measuring "coating only" properties using nanoindentation. In: Materials Research Society Symposium Proceedings, vol. 436, pp. 171–176 (1996)

13. Szlufarska, I.: Atomistic simulations of nanoindentation. Mater. Today **9**, 42–50 (2006)

14. Price, M., Ovcharenko, A., Thangaraj, R., Raeymaekers, B.: Deformation of ultra-thin diamond-like carbon coatings under combined loading on a magnetic recording head. Tribol. Lett. **57**(3), 1–9 (2015)

15. Szlufarska, I., Kalia, R., Nakano, A., Vashishta, P.: Nanoindentation-induced amorphization in silicon carbide. Appl. Phys. Lett. **85**, 378–380 (2004)

16. Szlufarska, I., Kalia, R., Nakano, A., Vashishta, P.: Atomistic mechanisms of amorphization during nanoindentation of SiC: a molecular dynamics study. Phys. Rev. B **71**, 174113 (2005)

17. Szlufarska, I., Kalia, R., Nakano, A., Vashishta, P.: Atomistic processes during nanoindentation of amorphous silicon carbide. Appl. Phys. Lett. **86**, 021915 (2005)

18. Szlufarska, I., Kalia, R., Nakano, A., Vashishta, A.: A molecular dynamics study of nanoindentation of amorphous silicon carbide. J. Appl. Phys. **102**, 023509 (2007)

19. Sinnott, S., Colton, R., White, C., Shenderova, O., Brenner, D., Harrison, J.: Atomistic simulations of the nanometer-scale indentation of amorphous-carbon thin films. J. Vac. Sci. Technol. A **15**, 936–940 (1997)

20. Wang, N., Komvopoulos, K.: Nanomechanical and friction properties of ultrathin amorphous carbon films studied by molecular dynamics analysis. ASME Conf. Proc. **2010**(44199), 393–395 (2010)

21. Deng, H., Minor, K., Barnard, K.: Comparison of mechanical and tribological properties of permalloy and high moment FeTaN thin films for tape recording heads. IEEE Trans. Magn. **32**, 3702–3704 (1996)

22. Ma, Z., Long, S., Pan, Y., Zhou, Y.: Creep behavior and its influence on the mechanics of electrodeposited nickel films. J. Mater. Sci. Technol. **25**, 90–94 (2009)

23. Frick, C., Clarck, B., Orso, S., Schneider, A., Arzt, E.: Size effect and strain hardening of small-scale [111] nickel compression pillars. Mater. Sci. Eng. A **489**, 319–329 (2008)

24. Klokholm, E., Aboaf, J.: The saturation magnetostriction of permalloy films. J. Appl. Phys. **52**, 2474–2476 (1981)

25. Gao, G., Mikulski, P., Harrison, J.: Molecular-scale tribology of amorphous carbon coatings: effects of film thickness, adhesion, and long-range interactions. J. Am. Chem. Soc. **124**, 7202–7209 (2002)

26. Baskes, M.: Modified embedded-atom potentials for cubic materials and impurities. Phys. Rev. B. **46**, 2727–2742 (1992)

27. Baskes, M., Angelo, J., Bisson, C.: Atomistic calculations of composite interfaces. Model. Simul. Mater. Sci. **2**, 505–518 (1999)

28. Tersoff, J.: New empirical approach for the structure and energy of covalent systems. Phys. Rev. B. **37**, 6991–7000 (1988)

29. Walsh, P., Omeltchenko, A., Kalia, R., Nakano, A., Vashishta, P., Saini, S.: Nanoindentation of silicon nitride: a multimillion-atom molecular dynamics study. Appl. Phys. Lett. **82**, 118–120 (2003)

30. Lide, D.: A survey of carbon–carbon bond lengths. Tetrahedron **17**, 125–134 (1962)

31. Plimpton, S.: Fast parallel algorithms for short-range molecular dynamics. J. Comput. Phys. **117**, 1–19 (1995)

32. Noreyan, A., Amar, J., Marinescu, I.: Molecular dynamics simulations of nanoindentation of β-SiC with diamond indenter. Mater. Sci. Eng. B **117**, 235–240 (2005)

33. Nair, A., Parker, E., Gaudreau, P., Farkas, D., Kriz, R.: Size effects in indentation response of thin films at the nanoscale: a molecular dynamics study. Int. J. Plast. **24**, 2016–2031 (2008)

34. Kikuchi, N., Kitagawa, M., Sato, A., Kusano, E., Nanto, H., Kinbara, A.: Elastic and plastic energies in sputtered multilayered Ti–TiN films estimated by nanoindentation. Surf. Coat. Technol. **126**, 131–135 (2000)

35. Fang, T., Wu, J.: Molecular dynamics simulations on nanoindentation mechanisms of multilayered films. Comput. Mater. Sci. **43**, 785–790 (2008)

36. Ma, Z., Long, S., Pan, Y., Zhou, Y.: Creep behavior and its influence on the mechanics of electrodeposited nickel films. J. Mater. Sci. Technol. **25**, 90–94 (2009)

37. Follstaedt, D., Knapp, J., Myers, S.: Mechanical properties of ion-implanted amorphous silicon. J. Mater. Res. **19**, 338–346 (2004)

38. Grill, A.: Diamond-like carbon: state of the art. Diam. Relat. Mater. **8**, 428–434 (1999)

39. Yasui, N., Inaba, H., Furusawa, K., Saito, M., Ohtake, N.: Characterization of head overcoat for 1 Tb/in^2 magnetic recording. IEEE Trans. Magn. **45**, 805–809 (2009)

40. Casiraghi, C., Robertson, J., Ferrari, A.: Diamond-like carbon for data and beer storage. Mater. Today **10**, 44–53 (2007)

41. Chen, X., Vlassak, J.: Numerical study on the measurement of thin film mechanical properties by means of nanoindentation. J. Mater. Res. **16**, 2974–2982 (2001)

42. Saha, R., Nix, W.: Effects of the substrate on the determination of thin film mechanical properties by nanoindentation. Acta Mater. **50**, 23–28 (2002)

43. Charitidis, C.: Nanomechanical and nanotribological properties of carbon-based thin films: a review. Int. J. Refract. Metals Hard Mater. **28**, 51–70 (2010)

44. Charitidis, C., Logothetidis, S., Gioti, M.: A comparative study of the nanoscratching behavior of amorphous carbon films grown under various deposition conditions. Surf. Coat. Technol. **125**, 201–206 (2000)

45. Li, J.: AtomEye: an efficient atomistic configuration viewer. Model. Simul. Mater. Sci. **11**, 173–177 (2003)